Evolution of the excited electron bubble in liquid ^{4}He and the appearance of fission-like processes

David Mateo, Martí Pi, and Manuel Barranco

Departament ECM, Facultat de Física, and IN2UB, Universitat de Barcelona, Diagonal 647, 08028 Barcelona, Spain

We have studied the evolution of an excited electron bubble in superfluid ^{4}He for several tens of picosecond combining the dynamics of the liquid with an adiabatic evolution for the electron. The path followed by the excited bubble in its decay to the ground state is shown to strongly depend on pressure. While for pressures below 1 bar the 1P excited electron bubble has allowance for radiatively decay to the deformed ground state, evolving then nonradiatively toward the ground state of the spherical electron bubble, we have found that above 1 bar two distinct baby bubbles appear in the course of the dynamical evolution, pointing to a different relaxation path in which the electron may be localized in one of the baby bubbles while the other collapses, allowing for a pure radiationless de-excitation. Our calculations are in agreement with experiments indicating that relaxed 1P bubbles are only observed for pressures smaller than a critical one, on the order of 1 bar, and that above this value the decay of the excited bubble has to proceed differently. A similar analysis carried out for the 2P bubble shows that the adiabatic approximation fails at an early stage of its dynamical evolution due to the crossing of the 2P and 1F states.

PACS number(s): 47.55.D−, 67.25.du, 33.20.Kf, 71.15.Mb

I. INTRODUCTION

Electron bubbles (ebubbles) in liquid helium are fascinating objects with an apparently simple structure that have been the subject of a large number of experimental and theoretical studies, see, e.g., Refs. [1–12] and references therein. The imaging of individual ebubbles moving in the liquid,[13] some unexplained events in cavitation experiments,[14] and the efforts in creating and detecting multielectron bubbles[15,16] are recent issues calling for a dynamical description of the electron bubble, but not the only ones. For instance, the equilibration of the electron bubble in superfluid liquid helium, studied in detail by Eloranta and Apkarian[8] within time-dependent density-functional (DF) theory, also needed of an accurate dynamical description. The ebubbles addressed in that work are spherically symmetric, which made the calculations affordable for using the best available DF for ^{4}He, the so-called Orsay-Trento functional.[17] Other dynamical studies have resorted to much simpler approaches inspired on local functionals of the kind proposed by Stringari and Treiner long time ago,[18] or on generalizations of the Gross-Pitaevskii equation to the description of liquid helium.[19–22] They have allowed to carry out dynamical studies involving nonspherical ebubbles, and their interaction with vortices in the superfluid. However, these local approaches do not describe the superfluid accurately. In particular, its elemental excitations are poorly reproduced. To circumvent this shortcoming, nonlocal extensions have been proposed[23] and applied, e.g., to vortex nucleation in superfluid helium.[24]

Another problem requiring a dynamical treatment, still not addressed in full detail, is the relaxation of an ebubble after being excited by photoabsorption, which constitutes the subject matter of this work. This process couples the fairly slow displacement of the helium bubble with the rapid motion of the electron it hosts, producing excitations in the liquid that take away a sizeable part of the energy deposited in

the ebubble during the absorption. The emission spectrum of the electron bubble after it has relaxed around the excited electron state has been calculated.[10,25,26] However, whether and how these full relaxed configurations are attained before decaying by photoemission was not elucidated.

In this work we attempt a theoretical description of the evolution of the excited ebubble based on the zero-temperature DF approach, using an as much accurate as technically feasible description of the liquid and an electron-helium (e-He) interaction that have been proved to reproduce the experimental absorption energies of the ebubble. The initial configuration is determined by a static calculation of the excited ebubble. This state has a large radiative lifetime, on the order of several tens of microsecond, in contrast with the short time scale for the helium displacement, on the order of picosecond. The subsequent dynamical evolution of the ebubble is described within the adiabatic approximation, which is valid for a period of time difficult to ascertain,[27] that we shall discuss in some detail. We will show that, depending on the initial excited state and the external pressure applied to the liquid, the bubble may keep its initial simply connected topology, or evolve toward a nonsimply connected one made of two baby bubbles that share the probability of finding the electron in,[28] the electron eventually localizing in one of them while the other collapses. To reduce the numerical effort to a reasonable amount, we shall mostly discuss results for the collapse of an ebubble starting from the spherical 1P state. Results for the collapse of the 2P state will be also shown.

This work is organized as follows. In Sec. II we describe our model and present a quasistatic study of the ebubble, completing the results we have presented elsewhere,[25] and recalling some technical details about the method we have used to solve the variational equations for the fluid and the electron. In Sec. III we present the adiabatic evolution of the ebubble for two selected values of the liquid pressure. The validity of the adiabatic approximation is analyzed in Sec. IV and a summary is presented in Sec. V.

II. QUASISTATIC DESCRIPTION

We first address some properties of excited electron bubbles in liquid ^{4}He using the Orsay-Trento density functional including the terms that mimic backflow effects and are crucial to quantitatively reproduce the experimental phonon-roton dispersion relation in bulk liquid ^{4}He at zero pressure.[17] They have no influence on the statics of the system and have been often neglected[12,29] in the dynamics because their inclusion makes the dynamical calculations very cumbersome.[8,30–32] In practice, we have found that these terms have little effect on the dynamics of the electron bubble presented in this work.

The e-He interaction has been modeled by the Hartree-type local effective potential derived by Cheng *et al.*[33] This allows us to write the energy of the electron-helium system as a functional of the electron wave function $\Phi(\mathbf{r})$ and the ^{4}He effective macroscopic wave function $\Psi(\mathbf{r}) = \sqrt{\rho(\mathbf{r})}\exp[\iota S(\mathbf{r})]$, where $\rho(\mathbf{r})$ is the particle density and $\mathbf{v}(\mathbf{r}) = \hbar \nabla S(\mathbf{r})/m_{\mathrm{He}}$ is the velocity field of the superfluid

$$E[\Psi,\Phi] = \frac{\hbar^2}{2m_{\mathrm{He}}}\int d\mathbf{r}|\nabla\Psi(\mathbf{r})|^2 + \int d\mathbf{r}\,\mathcal{E}(\rho)$$
$$+ \frac{\hbar^2}{2m_{\mathrm{e}}}\int d\mathbf{r}|\nabla\Phi(\mathbf{r})|^2 + \int d\mathbf{r}|\Phi|^2 V_{\mathrm{e\text{-}He}}(\rho). \quad (1)$$

In this expression, $\mathcal{E}(\rho)$ is the ^{4}He "potential" energy density and the e-He interaction $V_{\mathrm{e\text{-}He}}(\rho)$ is written as a function of the helium density.[33] Details are given in Refs. 9 and 34. In the absence of vortex lines, S is zero and E becomes a functional of ρ and Φ. Otherwise, one has to use the complex wave function $\Psi(\mathbf{r})$ to describe the superfluid.

For a given pressure (P), we have solved the Euler-Lagrange equations which result from the variation with respect to Ψ^* and Φ^* of the zero temperature constrained grandpotential density $\tilde{\omega}(\Psi,\Phi) = \omega(\Psi,\Phi) - \varepsilon|\Phi|^2$, with

$$\omega(\Psi,\Phi) = \frac{\hbar^2}{2m_{\mathrm{He}}}|\nabla\Psi(\mathbf{r})|^2 + \mathcal{E}(\rho) + \frac{\hbar^2}{2m_{\mathrm{e}}}|\nabla\Phi|^2 + |\Phi|^2 V_{\mathrm{e\text{-}He}}(\rho)$$
$$- \mu\rho, \quad (2)$$

where μ is chemical potential of the liquid. The variation of the above functional yields two coupled equations that have to be self-consistently solved

$$-\frac{\hbar^2}{2m_{\mathrm{He}}}\Delta\Psi + \left\{\frac{\delta\mathcal{E}}{\delta\rho} + |\Phi|^2\frac{\partial V_{\mathrm{e\text{-}He}}(\rho)}{\partial\rho}\right\}\Psi = \mu\Psi, \quad (3)$$

$$-\frac{\hbar^2}{2m_{\mathrm{e}}}\Delta\Phi + V_{\mathrm{e\text{-}He}}(\rho)\Phi = \varepsilon\Phi, \quad (4)$$

where ε is the eigenvalue of the Schrödinger equation obeyed by the electron.

Our method of solving the variational equations is based on a high-order discretization in Cartesian coordinates of the differential operators entering them (13-point formulas in the present case), and the use of fast Fourier transformation techniques[35] to efficiently compute the convolution integrals in $\omega(\rho)$, such as the mean-field helium potential and the coarse-grained density entering the definition of the correla-

tion energy.[12] This allows us to use a large spatial mesh step, of about 1 Å size, without an apparent loss of numerical accuracy when we compare our results with others (see below) obtained using three-point formulas for the derivatives that, as a consequence, require a rather small mesh step to be accurate. The density at the boundary of the three-dimensional $140 \times 140 \times 140$ Å^3 box used to carry out the calculations is fixed to the value of the bulk liquid density at the given P. We recall that knowledge of $\mathcal{E}(\rho)$ allows to determine the equation of state of the bulk liquid and its chemical potential, since $\mu = \partial\mathcal{E}/\partial\rho$ and $P = -\mathcal{E}(\rho) + \mu\rho$. Equations (3) and (4) have been solved employing an imaginary-time method,[36] and we have carried out the appropriate tests to check the stability of the solutions. We mention that the energies we have obtained for the 1S$\rightarrow$1P and 1S$\rightarrow$2P transitions[9] are in very good agreement with experiment,[6] and that our results compare well with those obtained by Eloranta and Apkarian[8] using the same functional but a different numerical method and e-He interaction. This constitutes an excellent test not only for the numerics but also for the physical ingredients employed in both calculations. We have recently discussed the effect of the presence of vortices on the absorption spectrum of ebubbles attached to them.[25]

Upon excitation to the 1P state by light absorption, the ebubble experiences a drastic change in shape. This is due to the fairly large radiative lifetime of this state (calculated to be 44 μs in Ref. 26, 60 μs in Ref. 10, and 56 μs in Ref. 25) as compared to any characteristic helium time scale, allowing the liquid to relax around the excited state. As a consequence, the bubble adapts its shape to the 1P electron probability density before decaying by photoemission to the deformed 1S state. Consequently, the bubble configuration at the emission time can be obtained by minimizing the grand-potential of the system keeping the electron in the excited 1P state. We have done it by solving Eqs. (3) and (4) taking for Φ the Φ_{1P} wave function. In this case, a Gram-Schmidt scheme has been implemented to determine both 1P and 1S relaxed states that obviously no longer correspond to a spherical bubble. In this axially symmetric environment, the spherical nL states are split depending on the value (m) of the orbital angular momentum on the symmetry z axis, and the $\pm m$ states are degenerate. We have found that, within a nL manifold, the m states are ordered in increasing $|m|$ values.[25] For this reason, we will refer to the axially symmetric state that corresponds to the $m = 0$ submanifold when we speak of a deformed "nL" state. When needed, we shall use the conventional notation for the orbital angular momentum of single-particle states in linear molecules, namely, $\sigma, \pi, \delta, \phi, \dots$ for $|m| = 0, 1, 2, 3, \dots$, and superscripts $+(-)$ for specularly symmetric (antisymmetric) states.

Figure 1 displays quasiequilibrium ebubble configurations at different stages of the absorption-emission cycle obtained at $P = 0$ bar. The electron-probability densities are represented by colored clouds, these with one lobe correspond to 1S states (spherical bubble, picture 1; deformed bubble, picture 4) and these with two lobes correspond to 1P states (spherical bubble, picture 2; deformed bubble, picture 3). In this figure, the line indicates the bubble dividing surface, i.e., the surface at which the liquid density equals half the
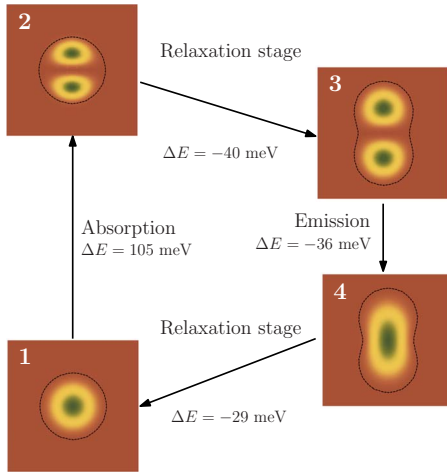
FIG. 1. (Color online) Ebubble quasiequilibrium configurations at different stages of the absorption-emission cycle corresponding to $P=0$ bar. The electron-probability densities are represented by colored clouds. The dashed line is the bubble dividing surface. The size of the frames is 70×70 Å^2.

saturation-density value ρ_0, e.g., 0.0218 Å^{-3} at $P=0$ bar, and represents the surface of the helium bubble. We have found[25] that at $P=0$ bar, the 1P→1S emission energy is 36 meV, close to the 35 meV found in Ref. [10], constituting another excellent test of the theoretical framework used by us and by these authors. The energy released in the optical 1S-1P absorption-emission cycle can be determined combining the results we have obtained in previous works.[9,25] For instance, at $P=0$ bar the released energy is 69 meV (compare with the 76 meV obtained in Ref. [10]). This energy is transferred to the superfluid through generation of different kind of excitations.

Quasiequilibrium configurations of the ebubble relaxed around the 1P state are shown in Fig. 2 for several P values. In this figure, helium is represented by warm colors and the electron-probability density (arbitrary units) by cool colors. The relaxation of the bubble around the 1P state produces a characteristic two-lobe peanut structure whose waist—or
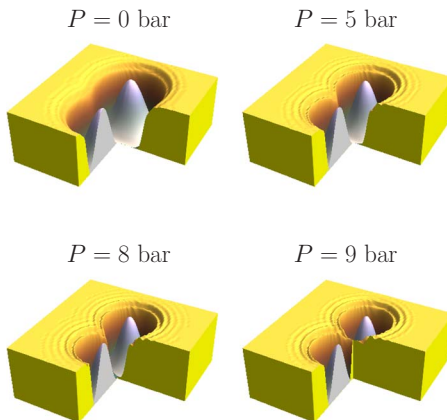
FIG. 2. (Color online) 1P bubble quasiequilibrium configurations for $P=0$, 5, 8, and 9 bars. Helium is represented by warm colors and the electron-probability density (arbitrary scale) by cool colors. The size of the samples is 70×70 Å^2.

neck—is progressively marked as the pressure applied to the liquid increases. Notice that helium displays a stratified density around the bubble. This feature appears whenever the superfluid presents a kind of free surface, as in drops, films or bubbles.[9,17,36]

Figure 2 shows that at a pressure of ~8 bars helium starts to penetrate between the two lobes of the electron wave function. At ~9 bars the helium density in this region reaches the saturation density, and the bubble splits into two baby bubbles. This produces an abrupt change in the emission energy, falling an order of magnitude between $P=8$ and 9 bars; in the "broken-neck" region extending up to the solidification pressure, the photon-emission energy is barely ~1 meV.[25] This is expectable at these pressures, as the main difference between 1S and 1P probability densities appears in the waist region. If this region is inaccessible to the electron due to the presence of helium, these states become almost degenerate. On the contrary, if this region is not accessible to the superfluid due, e.g., to the presence of a vortex whose vorticity line coincides with the symmetry axis of the ebubble, the baby bubbles may be held together by a tiny neck.[25]

It is worth pointing out that some of the quasiequilibrium configurations displayed in Fig. 2 may not be reachable in the evolution of the bubble. The reason is that helium falling in the waist region during the violent collapse may produce a large pileup of superfluid in that region, thus causing the actual breaking of the neck at pressures much smaller than the 8 bars obtained quasistatically. This possibility has been anticipated by Maris.[2]

III. TIME EVOLUTION OF THE EBUBBLE: PICOSECOND DYNAMICS

The dynamics of the excess electron localization in liquid helium has been adiabatically addressed by Rosenblit and Jortner[37,38] using a sharp-surface model for the bubble. The superfluid was considered as incompressible, and the bubble expansion time, i.e., the time for creating the ebubble, was estimated to be 8.5 ps when energy dissipation by emission of sound waves was taken into account.[38] This process exhibits a marked P dependence, the higher the pressure the shorter the expansion time.

Later on, the incompressibility approximation was relaxed using a DF approach, finding that at $P=0$ bar the bubble surface breathes with a period of about 130 ps.[8] These calculations have revealed that the localization process may launch shock waves, and that the subsequent main dissipation mechanism is sound radiation; excitations in the roton well were not produced.[8] In the present work we consider that the ebubble has had time enough to relax to its spherical 1S ground state and the electron is subsequently excited by light absorption to the 1P state, whose dynamical evolution is the subject matter of this section.

A. Adiabatic time evolution

Since the electron evolves much faster than helium as their mass ratio is $m_{He}/m_e \simeq 7300$, we have followed the dy-

namics of the excited ebubble by combining the actual time evolution of the liquid with an adiabatic evolution for the electron. Within this approximation, the electron wave function is found by solving, at each time step, the static Schrödinger Eq. (4) to obtain the instantaneous 1P electron state Φ_{1P}, and the structure of the liquid is obtained by determining the complex, time-dependent effective wave function $\Psi(\mathbf{r},t)$ from the time-dependent DF equation

$$\iota\hbar\frac{\partial\Psi(\mathbf{r},t)}{\partial t} = -\frac{\hbar^2}{2m_{He}}\Delta\Psi(\mathbf{r},t)$$
$$+\left\{\mathcal{U}[\rho,\mathbf{v}]+|\Phi_{1P}|^2\frac{\partial V_{e\text{-}He}(\rho)}{\partial\rho}\right\}\Psi(\mathbf{r},t), \quad (5)$$

where the effective potential $\mathcal{U}[\rho,\mathbf{v}]$ is given, e.g., in Refs. 30 and 31 and has an explicit dependence on the local current field $\mathbf{j}(\mathbf{r})=\rho(\mathbf{r})\mathbf{v}(\mathbf{r})$ arising from the backflow term the static potential energy in Eq. (1) lacks of. These coupled equations are solved imposing as initial conditions the stationary solution of the superfluid for the spherical 1S ebubble, employing the electron wave function Φ_{1P} for building the e-He interaction, as indicated in Eq. (5). The time step has been set to 0.01 ps, and we have used a fourth-order Runge-Kutta method to obtain the first time steps of the evolution. To determine the solution for subsequent times, we have used Hamming's (predictor-modifier-corrector) method.[39] This procedure is very robust and accurate, even for large amplitude motions.[40]

B. Results

We have solved the adiabatic-dynamic coupled equations for $P=0$, 0.5, 1, 2, 3, and 5 bars. We will mostly show results for the two extreme pressure values, namely, 0 and 5 bars. The evolution starts by stretching the bubble along the symmetry z axis and shrinking its waist. This produces density waves in the liquid that take away a sizeable part of the energy injected into the system during the absorption process, 105 meV at $P=0$ bar and 148 meV at 5 bars.[9]

The evolution can be safely followed for about 25–30 ps. For larger times, the density waves reflected on the box boundaries get back to the region where the bubble sits, spoiling the calculation. This time interval is large enough to see bubble splitting at the higher pressures. Otherwise, one needs to introduce a source of damping in the equation governing the liquid evolution [Eq. (5)], to prevent sound waves from bouncing back. Usually, introducing damping requires to enlarge the calculation box to accommodate a buffer region where waves are washed out, see, e.g., Refs. 8, 21, 22, and 41. This increases the number of grid points and slows the calculation.

Below 1 bar, we have found that the ebubble configuration is simply connected and radiates a sizeable part of the excitation energy as sound waves. For instance, at $P=0$ bar, the energy difference between the spherical 1P configuration and the relaxed 1P quasiequilibrium configuration is ~40 meV (see Fig. 1). The ebubble undergoes damped oscillations that will likely lead it to the corresponding quasistatic 1P configuration described in Sec. II. As a consequence, it would eventually decay radiatively to the deformed 1S state that will radiationless evolve toward the spherical 1S state.
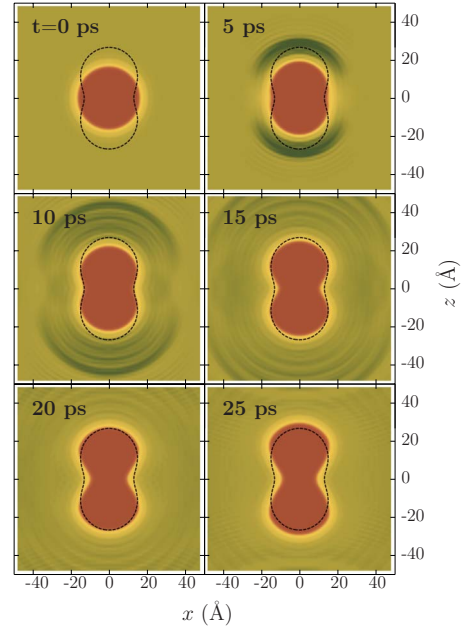
An example of this sort of evolution is shown in Fig. 3 for $P=0$ bar. We have found that after 15 ps, the shape of the 1P bubble is similar to the quasistatic configuration referred to in Sec. II. Using a simpler model, Maris has found a smaller value, 11 ps.[2] The difference is a natural consequence of the two basic approximations he has made, namely, treating the liquid as incompressible and neglecting sound-wave radiation. Due to the inertia of the bubble in the expansion process, it continues to stretch in the direction of the symmetry axis. This dilatation in the z direction goes on for the largest times we have followed the evolution (30 ps), accompanied by the appearance of a more marked neck.

At 1 bar, the neck collapses due to the large kinetic energy of the liquid filling in the region between the two 1P lobes, and the ebubble configuration becomes nonsimply connected. This causes the deformed 1P and 1S levels to become nearly degenerate, and their probability densities are almost identical. The appearance of any asymmetric fluctuation, which is beyond the scope and capabilities of our framework, will cause the electron to eventually localize in either of the baby bubbles. The subsequent evolution of the system is the collapse of the empty baby bubble and the evolution of the other one toward the spherical 1S ground state. In this case, the excited 1P bubble decays to the 1S spherical configuration without passing through the 1P quasistatic configuration described in the previous section, and the de-excitation is nonradiative. An example of this sort of evolution is shown in Fig. 4 for $P=5$ bars. For this pressure, we have found that a configuration similar to the simply

FIG. 3. (Color online) Adiabatic evolution of the 1P ebubble at $P=0$ bar. The panels display the helium configurations corresponding to 0, 5, 10, 15, 20, and 25 ps. The dashed line represents the dividing surface of the quasiequilibrium configuration at $P=0$ bar shown in Fig. 2.
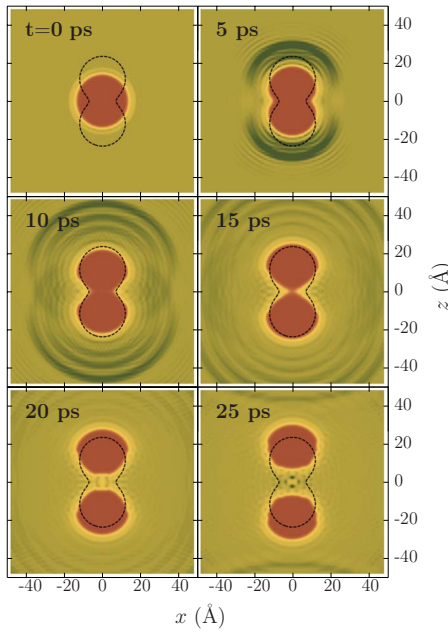
FIG. 4. (Color online) Adiabatic evolution of the 1P ebubble at $P=5$ bars. The panels display the helium configurations corresponding to 0, 5, 10, 15, 20, and 25 ps. The dashed line represents the dividing surface of the quasiequilibrium configuration at $P=5$ bars shown in Fig. 2.

connected quasistatic one is attained after 10 ps, although the inertia of the bubble expansion breaks the quasistatic neck at about 18 ps. The density pileup in the neck region continues and at about 22 ps the helium density in this region has a peak of $\sim 2\rho_0$, whose relaxation pushes the two baby bubbles in opposite directions helping the fission process.

Our calculations are in agreement with cavitation experiments[42] indicating that relaxed 1P bubbles are only produced for pressures smaller than about 1 bar, and that above this value the decay of the excited bubble has to proceed differently, likely radiationless. Indeed, we have found that the 1P bubble fissions at $P=1$ bar, but it does not at $P=0.5$ bar. Our results are also in agreement with the interpretation[27] of the vanishing of the photoconductivity signal below 1 atm experimentally observed by Grimes and Adams.[6] According to this interpretation, an ebubble in the 1P state is unstable against a radiationless de-excitation back to the ground state, the electron ultimately settling into one of the baby bubbles while the other collapses with phonon (heat) emission. It is this released heat that drives the photocurrent. Below that pressure, the ebubble decays radiatively, it does not release enough heat and is not detected in the photocurrent experiment.

The evolution of the electron energies for the 1S (empty) and 1P (occupied) states, together with a representation of the electron-probability densities, is presented in Fig. 5 for two pressure values. The fission of the bubble at $P=1$ bar happens after 60 ps. To obtain this result, we have proceeded as in Refs. 21 and 22, introducing a damping term in Eq. (5). To make sure that the bubble does not fission at $P=0.5$ bar, we have also introduced a damping term for this pressure.

We have studied the excitations produced in the liquid by the expansion of the ebubble. From the evolution of the first
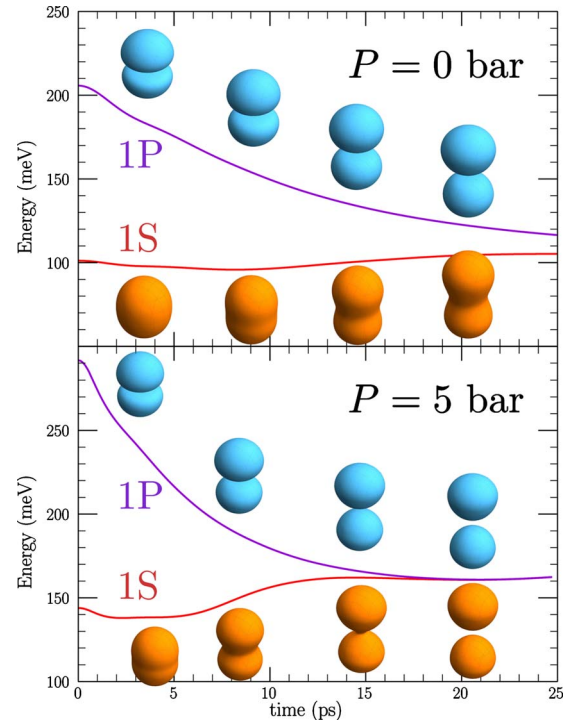
FIG. 5. (Color online) Adiabatic evolution of the energies of the 1S (empty) and 1P (occupied) states, together with a representation of the electron-probability densities for $P=0$ bar (top panel) and $P=5$ bar (bottom panel). The electron-probability densities are also displayed at four selected time values.

wave front, we have estimated that it moves in the z direction at ~ 330 m/s at $P=0$ bar and at ~ 410 m/s at $P=5$ bars. These values are well above the speed of sound in helium at these pressures, meaning that the dynamics is highly nonlinear. Besides, we have determined the nature of these excitations by Fourier analyzing the density waves along the z axis, leaving aside the region near the bubble surface. The density profile is shown in the top panel of Fig. 6, corresponding to $P=0$ bar at 13 ps, and the Fourier transform of the density fluctuation (related to the static structure function of the liquid) is presented in the bottom panel. Apart from the low-q component, arising from the mean-density profile, one can identify two distinct peaks, the more marked one at $q \sim 0.8$ Å^{-1} in the phonon branch near to the maxon region, and another at $q \sim 2.3$ Å^{-1} slightly to the right of the roton minimum. A similar "roton" peak was found in Ref. 8. A less marked peak appears at $q \sim 1.7$ Å^{-1}, slightly to the left of the roton minimum. Similar peaks have been found for shorter and larger times. From the relative intensity of these peaks, we are prone to identify most of the emitted waves as high-energy "phonons."

We have also analyzed the effect of the backflow term on the appearance of the density waves. One can see from the bottom panel of Fig. 6 that neglecting this term changes a little the relative intensity of the phonon and roton peaks, increasing the former and decreasing the later as expected from the effect of the backflow term on the excitation modes of the superfluid, see Fig. 12 of Ref. 17. We want to stress that rotons are not excited if one uses a less accurate, local
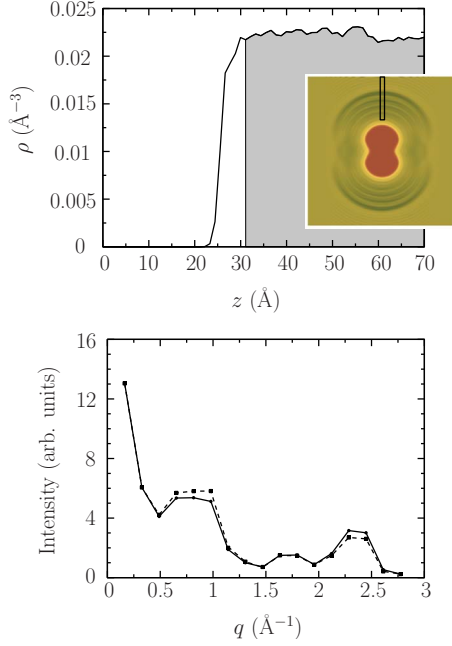
FIG. 6. (Color online) Top panel: density profile of the super-fluid corresponding to $P=0$ bar at 13 ps (only the $z \geq 0$ part is shown). The inset shows the ebubble configuration in a 140 $\times 140$ Å² frame, and the region displayed in the rectangle is the Fourier transformed one. Bottom panel: solid line, Fourier trans-form of the superfluid density profile shown in gray in the top panel. The dashed line is the Fourier transform of the density ob-tained at the same evolution time without including backflow ef-fects. In both cases the peak at $q=0$ Å^{-1} arises from the mean-density profile, not subtracted from the local density before transforming. The lines have been drawn as a guide to the eyes.

functional such as that of Refs. [18]–[22]. In this case, only the low-q phonon spectrum of the superfluid is quantitatively reproduced. Whether this has a sizeable influence on the ebubble dynamics or not, can only be ascertained by a de-tailed comparison between the results obtained using both kind of functionals.

1P ebubbles may be excited by photoabsorption to the 1D state, either to its $m=0$ component ($2\sigma^+$) or to its $m=\pm 1$ components ($1\pi^-$). The absorption spectrum at different stages of the time evolution can be measured in a pump-probe experiment by which the ebubble is excited by two consecutive laser pulses. The delay set between these pulses should correspond to the time elapsed between the excitation of the spherical bubble and the time at which the absorption spectrum of the 1P ebubble is recorded. Time-resolved elec-tronic spectroscopy has been proposed by Rosenblit and Jortner[38] as a tool for the exploration of the localization dy-namics of the excess electron.

Time-resolved excitation energies are shown in Fig. 7 at $P=0$ and 5 bars. While the evolution of the $1\sigma^- \rightarrow 1\pi^-$ ex-citation is qualitatively similar at both pressures, the $1\sigma^- \rightarrow 2\sigma^+$ excitation evolves differently in the high-pressure re-gime when the bubble splits. Indeed, at 0 bar the excitation energy smoothly decreases with time, whereas at 5 bars it starts decreasing, increasing next, and eventually becoming larger than the excitation energy to the $1\pi^-$ state. Note that
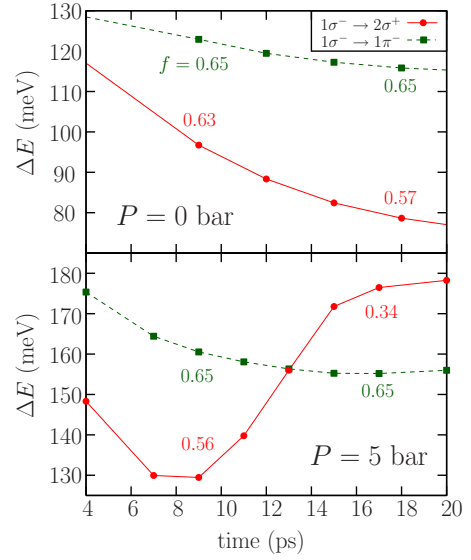
FIG. 7. (Color online) Time-resolved excitation energies at P $=0$ and 5 bars for electron transitions from the $1\sigma^-$ state arising from the spherical 1P, $m=0$ one, to either the $1\pi^-$ state (circles), or to the $2\sigma^+$ one (squares), both initially belonging to the spherical 1D manifold. In each panel, the oscillator strength for two selected time values is also displayed. Lines have been drawn as a guide to the eyes.

both the change in behavior and the crossing take place some picosecond before bubble splitting.

The $1\sigma^- \rightarrow 1\pi^-$ transition is little affected by bubble split-ting because it involves two states with negative specular symmetry, which means that the probability density of both states is zero in the neck region. On the contrary, the $1\sigma^- \rightarrow 2\sigma^+$ transition involves two states with different specular symmetry and thus it is more affected by bubble splitting.

Along with the excitation energies, some values of the associated oscillator strengths are displayed in Fig. 7. The oscillator strengths have been calculated in the dipole ap-proximation as[43]

$$f_{ab} = \frac{2m_e}{3\hbar^2}(E_a - E_b)|\langle a|\mathbf{r}|b\rangle|^2.$$

As known, the oscillator strengths fulfill a sum rule that in the one-electron case is $\Sigma_a f_{ab}=1$.[44] At both pressures, we have found that these transitions have comparable oscillator strengths. The largest difference appears for $P=5$ bars in the split-bubble regime. In it, the strength of the $1\sigma^- \rightarrow 2\sigma^+$ tran-sition is roughly half that of the $1\sigma^- \rightarrow 1\pi^-$ transition. We thus conclude that the analysis of the peak energy and oscil-lator strength of the $1\sigma^- \rightarrow 2\sigma^+$ transition might disclose the fission-like behavior of the excited 1P bubble, complement-ing the experimental information gathered from cavitation and photoconductivity experiments.

The current field $[\mathbf{j}(\mathbf{r})=\rho(\mathbf{r})\mathbf{v}(\mathbf{r})]$ is shown in Fig. 8 for $P=0$ and 5 bars at 12 and 22 ps. At 12 ps the current fields are qualitatively similar for both pressures: the bubble ex-pands along the symmetry axis and shrinks in a plane per-pendicular to it. At 22 ps, when $P=5$ bars, large currents keep bringing liquid into the neck region, splitting the bubble
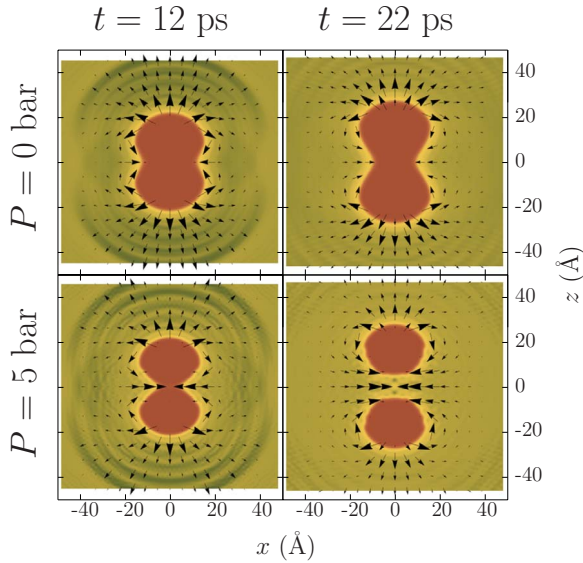
FIG. 8. (Color online) Current field at $P=0$ bar (top panels) and 5 bars (bottom panels) at time $t=12$ ps (left) and $t=22$ ps (right). In each panel, the larger the arrow, the larger the current.

and producing important density oscillations in the central region.

We have also followed the collapse of the 2P bubble at $P=0$ bar. About 2 ps after the collapse has started, a sizeable part of the excitation energy has been released into the liquid and two waves are distinguishable around the bubble, as shown in Fig. 9. These waves travel through the liquid at the same speed as in the 1P bubble case, ~ 330 m/s. Shortly after 7 ps, the $m=0$ levels of the 2P and 1F states become very close and, as discussed in the next section, see Eq. (7), the adiabatic approximation fails. At this point, the 2P bubble displays an incipient four-lobe shape arising from a similar structure in the 2P electron probability density. It is worth mentioning that a likely related effect, namely, the near degeneracy of the 2P and 1F states, was found in the quasistatic calculations of Ref. 26 as P increased.

In view of the mentioned failure and the lacking of experimental information on the collapse of the 2P bubble, we
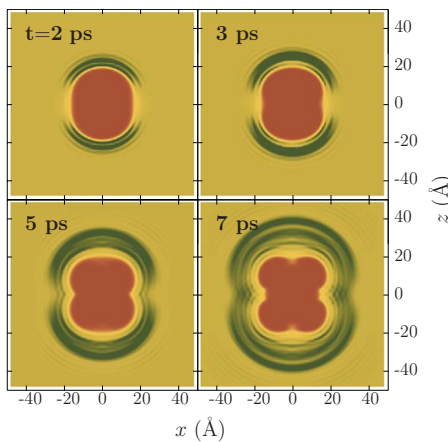
FIG. 9. (Color online) Adiabatic evolution of the 2P ebubble at $P=0$ bar. The panels display the helium configurations corresponding to 2, 3, 5, and 7 ps.

have closed its study at this point, leaving it for future work.

IV. VALIDITY OF THE ADIABATIC APPROXIMATION

The validity of the adiabatic approximation in the first stages of the bubble collapse, when the topology of the bubble is simply connected, stems from the very different time scale of the electron motion as compared to that of the bubble,[45] represented by the period of its shape oscillations. If the fluid is incompressible and the bubble spherical, the surface λ modes of the cavity are at energies

$$\hbar\omega_\lambda = \sqrt{\frac{\gamma}{m_{\mathrm{He}}\rho_0 R^3}(\lambda-1)(\lambda+1)(\lambda+2)}, \qquad (6)$$

where γ and ρ_0 are the surface tension and atom density of the liquid, respectively. For $\lambda=2$ this energy is about 1 K, and the period of the oscillation is ~ 50 ps.

The situation may change in the course of the collapse because the energy difference $\Delta = E_{1\mathrm{P}} - E_{1\mathrm{S}}$ between the deformed states decreases and the time scale $\tau = h/\Delta$ may become similar to the period of the shape oscillations of the deformed bubble. Since Δ is small in the two bubble regime, the approximation likely fails there.[27,46] It is worthwhile mentioning that neck fluctuations, not included in our approach nor in previous works, would pinch off the bubble at earlier stages of the collapse, in a similar way as they may cause the prompt scission of the fissioning atomic nucleus after the saddle configuration has been overcome.[47]

On the light of our model, in which no assumptions are made on the shape of the bubble nor the impenetrability of the bubble surface by the localized electron, it is instructive to analyze the validity of the adiabatic approximation assuming that, during the evolution, the bubble keeps its original axial symmetry and specular symmetry about the plane perpendicular to the symmetry axis that contains the node of the 1P state. This excludes any possible fluctuation and the appearance of asymmetric modes, like the breathing mode discussed in Ref. 27. Our discussion relies on the detailed presentation by Messiah,[48] that we summarize in the following.

The subsystem to which the adiabatic approximation is applied is the electron, whose wave function is decoupled from that of the liquid. This wave function evolves in the potential field generated by the liquid distribution, and its Hamiltonian is time dependent, $\mathcal{H}_e(t) = \mathcal{H}_e[\rho_{\mathrm{He}}(t)]$. Let ϕ_n^t be an eigenfunction of the Hamiltonian at time t, so that $\mathcal{H}_e(t)\phi_n^t = \varepsilon_n(t)\phi_n^t$. If $\phi_n(t)$ is the actual wave function ϕ_n^0 evolved up to time t, one has $\phi_n(t) = \mathcal{U}(t)\phi_n^0$, where $\mathcal{U}$ is the evolution operator. In the adiabatic approximation, one identifies $\phi_n(t)$ with ϕ_n^t, the intuitive justification being that if one perturbes the subsystem slowly and gently enough, it has enough time to adapt itself to the new environment "with no inertia" from the past configuration.

The error made in this approximation for a given state $|i\rangle$—the validity of the adiabatic approximation is assessed for a given state of the subsystem, not necessarily for them all—is defined as the probability of finding the subsystem in a state different from the initial one evolved in time within the "true" dynamics, $\eta_{ij} = |\langle \phi_j^t | \mathcal{U}(t) | \phi_i^0 \rangle|^2$. This error can be written in a workable way as[48]

$$\eta_{ij}(t) = \left| \frac{\hbar}{[\varepsilon_j(t) - \varepsilon_i(t)]^2} \langle \phi_j^t | \frac{d\mathcal{H}_e}{dt} | \phi_i^t \rangle \right|^2. \qquad (7)$$

If $\eta_{ij} \ll 1 \, \forall \, i \neq j$, the adiabatic approximation is justified. It is usually understood that it breaks down when the levels get very close or when they cross each other. Notice, however, that this assumes that these states can be connected by the evolved Hamiltonian. If a symmetry is dynamically conserved (in our case, angular momentum and specular symmetry are), then the adiabatic evolution of states with a given quantum number associated to this symmetry is not perturbed by states with different values of this quantum number. Although sometimes ignored, this is a very reasonable statement.

In the case of the $1\sigma^-$ state arising from the spherical 1P manifold, the adiabatic approximation holds even when its energy becomes almost identical to the energy of the $1\sigma^+$ state arising from the spherical 1S one, i.e., a small Δ does not invalidate the adiabatic approximation. The closest state having the same angular momentum and specular symmetry is the $2\sigma^-$ one arising from the spherical 1F manifold. At $P=5$ bars, we have found that these two states are 2000 K apart in the 10–20 ps range. Since $\hbar \sim 7.6$ K ps, one has $\hbar/(E_{2\sigma^-} - E_{1\sigma^-})^2 \sim 2 \times 10^{-6}$ ps K^{-1}. The value of the matrix element in Eq. (7) is some tens of kelvin per picosecond, so that the adiabatic approximation would be fulfilled even for the configuration displayed in Fig. 4 at 25 ps. Indeed, we have calculated η in the above time range and have found that it is on the order of 10^{-8}.

It is also worth analyzing the stability of the quasiequilibrium configurations when the symmetries are not exactly conserved because of perturbations from the environment. In this situation, let us assume that when the bubble splits the electron localizes in one of the lobes. Leaving out the discussion on the actual localization process, we have tried to infer the likely evolution of an ebubble with a localized electron. The localized electron state in either baby bubble is approximated by

$$\Phi_\pm = \frac{1}{\sqrt{2}} \phi_{1S} \pm \frac{1}{\sqrt{2}} \phi_{1P}. \qquad (8)$$

Consider now a short-time dynamics in which the liquid is kept frozen. The evolution of, e.g., the Φ_+ localized state is an oscillation between the two lobes

$$\Phi(t) = e^{-iE_{1S}t/\hbar}[\cos(\omega t)\Phi_+ - i\sin(\omega t)\Phi_-], \qquad (9)$$

where $\omega = (E_{1P} - E_{1S})/\hbar$. If this frequency is large enough, the liquid cannot react to the localization of the electron in either lobe and will essentially behave as if the electron were delocalized.

The time elapsed between two consecutive localizations of the electron in a given baby bubble is $\tau = \pi/\omega$. The value of this period as a function of pressure for the quasiequilibrium configurations is displayed in Fig. 10. In the split-bubble regime ($P \gtrsim 9$ bars), this period is of several picosecond, indicating that the electron-localization dynamics into one of the baby bubbles is not a trivial process to address.

$$\phi_+ = \frac{1}{\sqrt{2}}\phi_{1S} + \frac{1}{\sqrt{2}}\phi_{1P}$$
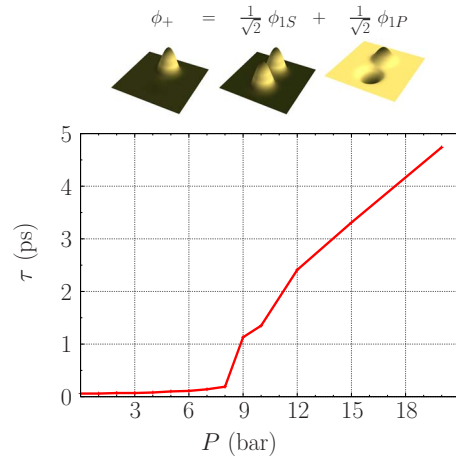
FIG. 10. (Color online) Top: superposition of the 1S and 1P states corresponding to the quasiequilibrium configuration at $P=9$ bars to approximately localize the electron in one of the baby bubbles. Bottom: tunneling period of a localized electron in one of the lobes of the quasiequilibrium ebubble as a function of pressure.

The electron will bounce back and forth as the liquid tries to adapt to it. Real-time calculations are thus needed to describe electron localization.

It is clear that the previous discussion on the validity of the adiabatic evolution lacks for incorporating fluctuations or excitations of low-energy modes that may appear in the course of the bubble evolution and couple the 1P and 1S states that otherwise are not, as previously discussed. One such mode has been thoroughly addressed by Elser:[27] a peanut configuration, whose walls are impenetrable by the electron, is represented by two intersecting sharp spheres of radius R_2 (instead of the deformed baby bubbles displayed in Fig. 4) joined along a circular orifice of radius a. These spheres are breathing in counterphase, producing an antisymmetric mode whose stiffness $\mathcal{K}$ and inertia $\mathcal{M}$ can be obtained analytically. This mode is very appealing, as it represents a small, swifting imbalance of the symmetric electron-probability density.

In the harmonic limit, if $a \ll R_2$, the stiffness and inertia of the asymmetric mode are[49]

$$\mathcal{K} = 16\left[\frac{E_0^2}{R_2^2 \Delta} + \pi(\gamma + R_2 P)\right],$$

$$\mathcal{M} = 4\pi\xi m_{4\text{He}}\rho_0 R_2^3. \qquad (10)$$

In these equations, $E_0 = \gamma R_0^2 \sim 9$ meV represents the energy unit with $\gamma = 2.36 \times 10^{-2}$ meV Å^{-2} being the surface tension of the liquid, $R_0 \sim 20$ Å is the radius of the spherical bubble, $R_2 \sim 16$ Å is the radius of the baby bubbles, $\xi \sim 1.70$ is a dimensionless constant, and $\Delta = E_{1P} - E_{1S}$. The frequency of the antisymmetric breathing mode is given by $\omega_{AB} = \sqrt{\mathcal{K}/\mathcal{M}}$, and the radius of the orifice is[27]

$$\Delta = \frac{4\pi}{3} E_0 \left(\frac{R_0}{R_2}\right)^2 \left(\frac{a}{R_2}\right)^3. \qquad (11)$$

The adiabatic approximation fails when $\omega_{AB} \simeq \Delta/\hbar$. This yields $\Delta \sim 0.14$ meV in the $P=0-5$ bars range, as only the first term in the stiffness turns out to be relevant in this regime. Thus, keeping only the first term in $\mathcal{K}$, one gets[50]

$$\frac{a}{R_2} = \left[\left(\frac{27}{8\pi^4\xi}\right) \left(\frac{m_e}{m_{He}\rho_0 R_0^3}\right) \left(\frac{R_2}{R_0}\right) \right]^{1/9} \sim 0.13. \qquad (12)$$

Hence, $a \sim 2.1$ Å. Clearly, such analytical results cannot be obtained within the DF approach, but we can use them to determine whether the dynamic and static configurations shown in Secs. II and III are reliable.

The adiabatic approximation thus holds at $P=0$ bar, as the neck radius is fairly large, see Fig. 3, and Δ is always much larger than 0.14 meV, see Fig. 5. From Fig. 4 we also conclude that, at $P=5$ bars, the adiabatic approximation is valid up to nearly the collapse of the waist. Indeed, the neck radius of the helium configuration at about 17–18 ps is ~ 2 Å, see Fig. 4. It is worth noting the difficulty in defining an effective radius for the orifice when the surface of the bubble is diffuse; we recall that the surface thickness of a ^{4}He drop of $10^3 - 10^4$ atoms is some $6-8$ Å.[51] Note also that the surface thickness of the helium bubble is rather independent of the curvature of the surface, as can be inferred from the fairly constant bright region around the bubbles displayed in Figs. 3 and 4.

Since we do not treat the bubble as impenetrable to the excess electron, the relation between the actual Δ and a values should not exactly be as given by Eq. (11). Using the result $\hbar\omega_{AB} \leq \Delta = 0.14$ meV as a criterion for the applicability of the adiabatic approximation instead of reaching the limiting value $a \sim 2$ Å, we find that the approximation holds up to 21 ps, when the bubble has already split into two baby bubbles. Both procedures indicate that when the adiabatic approximation likely fails, the baby bubbles have already developed.

The previous analysis leads us to conclude that, at high pressures, baby bubbles are formed some tens of picosecond after the starting of the collapse of the 1P bubble. From this point on, the likely fate of the system is the localization of the electron in one of the baby bubbles and the collapse of the other. This process is helped/triggered by fluctuations that break the specular symmetry of the ebubble configuration. As mentioned, determining the time scale of electron localization is beyond the capabilities of the adiabatic approximation. It has been calculated[21] that once the electron is localized, it takes to the superfluid some 20 ps to adapt to it while the other baby bubble is absorbed.

V. SUMMARY

Within density-functional theory, we have carried out an analysis of the adiabatic evolution of the excited electron bubble in superfluid liquid ^{4}He. We have found that for pressures below 1 bar, the 1P ebubble may relax to its quasistatic equilibrium configuration and decay radiatively to the deformed 1S state. This state evolves nonradiatively to the spherical 1S bubble, completing the absorption/emission cycle. This conclusion arises, in part, from studies carried out for 100 ps using a less accurate functional,[52] whose results qualitatively agree with ours for the first tens of picosecond.

At higher pressures, the situation drastically changes and the excited 1P bubble no longer decays to the quasistatic equilibrium configuration, whose physical realization is unlikely. Indeed, our analysis of the adiabatic approximation indicates that it is valid up to a point where two deformed, nearly disconnected baby bubbles appear in the dynamical evolution, pointing toward a fission-like de-excitation process, the likely subsequent evolution of the system being the localization of the electron in one of the baby bubbles and the collapse of the other. This collapse takes some 20 ps,[21] and the whole de-excitation process is radiationless.

We have also found a marked change in the behavior of the time-resolved absorption spectrum of the 1P bubble depending on whether the bubble fissions or not, i.e., on the liquid pressure. This change is, in principle, an experimentally accessible observable whose determination may complement the information obtained from cavitation and photoconductivity experiments.

Our analysis of the collapse of the 2P bubble has shown that the adiabatic approximation breaks down at an early stage of the dynamical process due to the crossing of 2P and 1F states. Although disclosed by the adiabatic approximation, this crossing has nothing to do with the approximation itself, but is inherent to the dynamics of the electron bubble. From the crossing point on, the bubble will relax around a mixed state with 2P and 1F components, and hence the physical realization of a pure quasiequilibrium 2P configuration is unlikely. It is very plausible that the same applies to other high-energy nL ebubbles generated in the absorption process. The possibility that some of them undergo a spontaneous symmetry breaking, as suggested by Grinfeld and Kojima[53] for the 2S state, can only reinforce our conclusion. Obviously, this does not question the existence of either relaxed quasiequilibrium configurations at low pressures or of baby bubbles at high pressures, arising from the evolution of the spherical 2P bubble. It just means that, on the one hand, the relaxed bubble will not be a pure 2P configuration and, on the other hand, to study the de-excitation of these bubbles one has to go beyond the adiabatic approximation and carry out a more demanding real-time dynamics calculation for the electron.

[1] M. Rosenblit and J. Jortner, J. Chem. Phys. **124**, 194505 (2006); **124**, 194506 (2006).

[2] H. J. Maris, J. Phys. Soc. Jpn. **77**, 111008 (2008).

[3] J. A. Northby and T. M. Sanders, Phys. Rev. Lett. **18**, 1184 (1967).

[4] W. B. Fowler and D. L. Dexter, Phys. Rev. **176**, 337 (1968).

[5] T. Miyakawa and D. L. Dexter, Phys. Rev. A **1**, 513 (1970).

[6] C. C. Grimes and G. Adams, Phys. Rev. B **41**, 6366 (1990).

[7] C. C. Grimes and G. Adams, Phys. Rev. B **45**, 2305 (1992).

[8] J. Eloranta and V. A. Apkarian, J. Chem. Phys. **117**, 10139 (2002).

[9] V. Grau, M. Barranco, R. Mayol, and M. Pi, Phys. Rev. B **73**, 064502 (2006).

[10] L. Lehtovaara and J. Eloranta, J. Low Temp. Phys. **148**, 43 (2007).

[11] B. DuVall and V. Celli, Phys. Rev. **180**, 276 (1969).

[12] M. Pi, R. Mayol, A. Hernando, M. Barranco, and F. Ancilotto, J. Chem. Phys. **126**, 244502 (2007).

[13] W. Guo, D. Jin, G. M. Seidel, and H. J. Maris, Phys. Rev. B **79**, 054515 (2009).

[14] A. Ghosh and H. J. Maris, Phys. Rev. Lett. **95**, 265301 (2005).

[15] J. Tempere, I. F. Silvera, and J. T. Devreese, Surf. Sci. Rep. **62**, 159 (2007).

[16] J. Fang, A. E. Dementyev, J. Tempere, and I. F. Silvera, Rev. Sci. Instrum. **80**, 043901 (2009).

[17] F. Dalfovo, A. Lastri, L. Pricaupenko, S. Stringari, and J. Treiner, Phys. Rev. B **52**, 1193 (1995).

[18] S. Stringari and J. Treiner, Phys. Rev. B **36**, 8369 (1987); J. Chem. Phys. **87**, 5021 (1987).

[19] N. G. Berloff and P. H. Roberts, Phys. Rev. B **63**, 024510 (2000); J. Phys. A **34**, 81 (2001).

[20] E. J. M. Madarassy and C. F. Barenghi, J. Low Temp. Phys. **152**, 122 (2008).

[21] D. Jin, W. Guo, W. Wei, and H. J. Maris, J. Low Temp. Phys. **158**, 307 (2010).

[22] D. Jin and H. J. Maris, J. Low Temp. Phys. **158**, 317 (2010).

[23] N. G. Berloff and P. H. Roberts, J. Phys. A **32**, 5611 (1999).

[24] N. G. Berloff and P. H. Roberts, Phys. Lett. A **274**, 69 (2000).

[25] D. Mateo, A. Hernando, M. Barranco, and M. Pi, J. Low Temp. Phys. **158**, 397 (2010).

[26] H. J. Maris, J. Low Temp. Phys. **132**, 77 (2003).

[27] V. Elser, J. Low Temp. Phys. **123**, 7 (2001).

[28] R. Jackiw, C. Rebbi, and J. R. Schrieffer, J. Low Temp. Phys. **122**, 587 (2001).

[29] F. Ancilotto, M. Barranco, and M. Pi, Phys. Rev. Lett. **91**, 105302 (2003).

[30] L. Lehtovaara, T. Kiljunen, and J. Eloranta, J. Comput. Phys. **194**, 78 (2004).

[31] L. Giacomazzi, F. Toigo, and F. Ancilotto, Phys. Rev. B **67**, 104501 (2003).

[32] F. Ancilotto, F. Dalfovo, L. P. Pitaevskii, and F. Toigo, Phys. Rev. B **71**, 104530 (2005).

[33] E. Cheng, M. W. Cole, and M. H. Cohen, Phys. Rev. B **50**, 1136 (1994); **50**, 16134 (1994) (erratum).

[34] M. Pi, M. Barranco, R. Mayol, and V. Grau, J. Low Temp. Phys. **139**, 397 (2005).

[35] M. Frigo and S. G. Johnson, Proc. IEEE **93**, 216 (2005).

[36] M. Barranco, M. Guilleumas, E. S. Hernández, R. Mayol, M. Pi, and L. Szybisz, Phys. Rev. B **68**, 024515 (2003).

[37] M. Rosenblit and J. Jortner, Phys. Rev. Lett. **75**, 4079 (1995).

[38] M. Rosenblit and J. Jortner, J. Phys. Chem. A **101**, 751 (1997).

[39] A. Ralston and H. S. Wilf, *Mathematical Methods for Digital Computers* (Wiley, New York, 1960).

[40] M. Barranco, R. Guardiola, S. Hernández, R. Mayol, J. Navarro, and M. Pi, J. Low Temp. Phys. **142**, 1 (2006).

[41] Ch. Cerjan, D. Kosloff, R. Kosloff, and M. Reshef, Geophysics **50**, 705 (1985).

[42] H. J. Maris, A. Ghosh, D. Konstantinov, and M. Hirsch, J. Low Temp. Phys. **134**, 227 (2004).

[43] M. Weissbluth, *Atoms and Molecules* (Academic Press, New York, 1978).

[44] Recall that if the initial state $|b\rangle$ is not the ground state, the sum includes negative terms arising from de-excitation transitions, hence a partial sum can be greater than unity.

[45] H. J. Maris, J. Low Temp. Phys. **120**, 173 (2000).

[46] A. I. M. Rae and W. F. Vinen, J. Low Temp. Phys. **123**, 1 (2001).

[47] U. Brosa, S. Grossmann, A. Müller, and E. Becker, Nucl. Phys. A **502**, 423 (1989).

[48] A. Messiah, *Quantum Mechanics* (North-Holland, Amsterdam, 1962).

[49] Since the asymmetric mode of Ref. 27 does not conserve the volume of the bubble, the stiffness slightly changes from the expression given in Ref. 27 if $P \neq 0$. In the numerical application we have used the $\gamma(P)$ law deduced in Ref. 9.

[50] This equation differs from Eq. (9) of Ref. 27 because of an error made there to obtain it from a straightforward combination of its Eqs. (3) and (8), as can be easily checked.

[51] J. Harms, J. P. Toennies, and F. Dalfovo, Phys. Rev. B **58**, 3341 (1998).

[52] D. Jin, W. Guo, W. Wei, and H. J. Maris (unpublished), and Ref. 21.

[53] P. Grinfeld and H. Kojima, Phys. Rev. Lett. **91**, 105301 (2003).